

Ultraweak-Absorption Microscopy of a Single Semiconductor Quantum Dot in the Midinfrared Range

Julien Houel,¹ Sébastien Sauvage,^{1,†} Philippe Boucaud,^{1,*} Alexandre Dazzi,² Rui Prazeres,² François Glotin,² Jean-Michel Ortéga,² Audrey Miard,³ and Aristide Lemaître³

¹*Institut d'Electronique Fondamentale CNRS, UMR8622, Université Paris-Sud, F-91405, Orsay, France*

²*CLIO-Laboratoire de Chimie Physique CNRS, UMR8000, Université Paris-Sud, F-91405, Orsay, France*

³*Laboratoire de Photonique et Nanostructures CNRS, Route de Nozay, F-91460, Marcoussis, France*

(Received 25 April 2007; published 20 November 2007)

We show that we can measure the room temperature ultraweak absorption of a single buried semiconductor quantum dot. This is achieved by monitoring the deformation field induced by the absorption of midinfrared laser pulses and locally detected with an atomic force microscope tip. The absorption is spectrally and spatially resolved around $\lambda \sim 10 \mu\text{m}$ wavelength with 60 nm lateral resolution ($\lambda/150$). The electronic *S-D* intersublevel absorption of a single quantum dot is identified around 120 meV and exhibits a homogeneous linewidth of ~ 10 meV at room temperature.

DOI: [10.1103/PhysRevLett.99.217404](https://doi.org/10.1103/PhysRevLett.99.217404)

PACS numbers: 78.67.Hc, 07.79.Lh, 73.21.La, 78.30.Fs

Semiconductor self-assembled quantum dots are key elements for optoelectronic devices or quantum information applications [1] and quantum dots charged with electrons are promising nanostructures for spin control and spin manipulation [2]. Monitoring and spatially resolving localized charges at the single quantum dot level is an important step for charge manipulation and coherent control experiments on these nanostructures. In the visible or near-infrared spectral range, photoluminescence combined with scanning near-field optical microscopy can provide high sensitivity and subwavelength spatial resolution down to a few tens of nm [3]. Another approach to optically study single quantum dots relies on transmission experiments by using coherent nonlinear spectroscopy coupled with the spatial selectivity of near-field spectroscopy [4] or by probing the absorption [5]. Single self-assembled quantum dots with lifetime limited linewidths can exhibit absorption amplitude up to 1.8% at low temperature in the near-infrared spectral range [6]. The spectral measurement of the absorption of single quantum dots has been reported for visible or near-infrared wavelengths in resonance with interband transitions involving electron and hole pairs. Only the high sensitivity obtained for optical measurements in the visible spectral range and nonlinear spectroscopy have allowed to achieve both spectral resolution and subwavelength spatial resolution of absorption [4]. These measurements were moreover performed at low temperature since the increase of homogeneous broadening from low temperature to 300 K leads to a drastic reduction by about 4 orders of magnitude of absorption amplitude as the temperature is increased. No successful attempt to measure single quantum dot absorption in the midinfrared spectral range has been reported at any temperature, even less with spatial and spectral resolution. Aperturless scanning near-field probing has been developed recently to obtain contrast from vibrational absorption with nanometer scale resolution (<100 nm) at $10 \mu\text{m}$ for surface patterns [7].

However, this scattering type approach mixes both the real and imaginary part of the refractive index, i.e., both the effect of spatial inhomogeneities and absorption. It also relies on strong absorbing layers, the significant infrared material contrast reported in Ref. [7] corresponding to absorptance in the percent range.

Charged self-assembled quantum dots with electrons or holes can be probed through their intersublevel absorption [8], corresponding in quantum dots to the intraband transition of a single charge between discrete confined levels originating from the same band (e.g., the conduction band). These transitions are resonant in the mid- or far-infrared spectral range and their energies depend on the quantum dot size, shape, and composition. InAs/GaAs self-assembled quantum dots with typical 20 nm in-plane dimension and typical 4 nm height exhibit conduction intersublevel transitions between 5–8 μm (bound-to-continuum transitions) and 8–20 μm (bound-to-bound transitions). The intersublevel absorptance amplitude at resonance of a single quantum dot containing one electron probed by a uniformly illuminated beam of section S is $\alpha = e^2 \omega_0 d^2 / c \varepsilon_0 n \hbar \Gamma S$, where e is the electronic charge, d the dipole length of the transition, $\hbar \omega_0$ the transition energy, c the light speed, ε_0 the vacuum permittivity, n the refractive index (3.3), $\Gamma = 1/T_2$ the dephasing rate. If a dipole length d of 0.35 nm [9], a typical $S = 25 \mu\text{m}^2$ diffraction limited illumination area, and a dephasing rate corresponding to a $2\hbar\Gamma = 10$ meV homogeneous broadening at room temperature are considered, the absorptance amplitude is as small as $\sim 3 \times 10^{-9}$ for a resonant intersublevel transition at $10 \mu\text{m}$ wavelength. Moreover, this wavelength corresponds to the spectral range of the strong ambient black-body background radiation. The measurement of this absorption therefore requires a highly sensitive technique.

We have resolved both spatially and spectrally the ultraweak absorption of buried single self-assembled quantum dots in the midinfrared. A schematic description of the

apparatus is depicted in Fig. 1. The setup is based on an atomic force microscope in the midinfrared (AFMIR) recently developed at the free-electron laser facility CLIO [10]. The *n*-doped InAs/GaAs self-assembled quantum dots were grown by molecular beam epitaxy with a $400 \mu\text{m}^{-2}$ sheet density (average dot distance of 50 nm) [11]. The doped quantum dots, buried 20 nm below the surface, are excited at room temperature by the infrared picosecond pulses of a free-electron laser. The energy absorbed by a single quantum dot is expected to be non-radiatively transferred to the lattice by the emission of optical phonons and their anharmonic decay into acoustical phonons [12]. The local thermal expansion generates a deformation field and launches a displacement impulse that propagates in a few ps towards the surface. The local surface displacement is probed by the gold-covered tip of an atomic force microscope operated in contact mode. The atomic force microscope (AFM) tip contact surface sets the lateral resolution down to the nanometer scale (tip radius is 200 nm, contact radius is ~ 2 nm). The strain pulses induce a percussional excitation of the AFM cantilever on a ps time scale, i.e., on a much smaller time scale than bulk heat diffusion. The energy provided by the picosecond pulse excitation is finally transferred to the low frequency vibration modes of the cantilever. The free-electron laser delivers pulse sequences ($8 \mu\text{s}$ length duration) at a repetition rate of 25 Hz, each of them containing picosecond pulses separated by 32 ns. The average incident power on the ZnSe prism is around 10 mW.

Figure 2(a) shows typical temporal deviation spectra of the AFM tip positioned out of and on a significantly populated single self-assembled quantum dot. The detection of this vibration, synchronously with the macropulse of the free-electron laser, is typically averaged 40 times. This signal is Fourier transformed in order to analyze spectrally the different vibration modes of the cantilever.

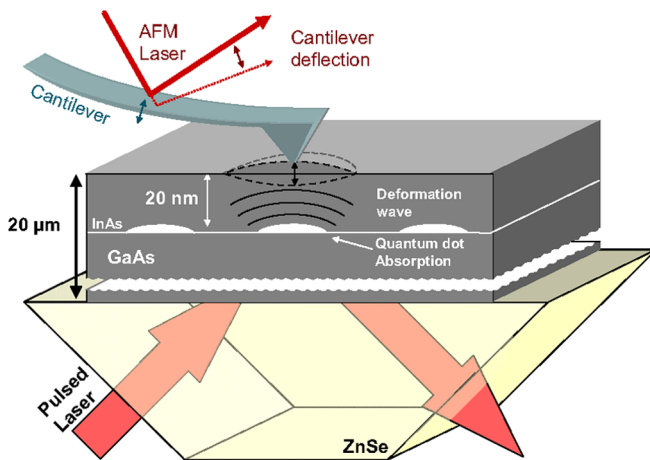


FIG. 1 (color online). Schematic description of the AFM experimental setup and operation principle for the room temperature measurement of the ultraweak absorption.

Figure 2(b) shows the power spectrum density of the Fourier transform of the cantilever deflection. For a V-shaped cantilever, three main vibration modes are observed in contact mode with resonances around 30 kHz, 50 kHz, and 60 kHz. The spectral resolution is 500 Hz. When the AFM tip is on top of an absorbing quantum dot, the amplitude of the signal changes significantly and its frequency is shifted towards higher energy. Both amplitudes and frequency shifts are a signature of the quantum dot absorption strength. The presence of buried charged quantum dots can therefore be monitored by detecting the vibration amplitude of the cantilever eigenmodes.

Figure 3(b) presents a two-dimensional $800 \times 800 \text{ nm}^2$ image of a quantum dot sample, sample S1, for which the electron population is provided by a $4 \times 10^{11} \text{ cm}^{-2}$ density Si delta-doping layer inserted 2 nm beneath the wetting layer. The excitation wavelength is $9.6 \mu\text{m}$. The value at each pixel of the image is obtained by integrating the signal over the vibrational modes of the cantilever (25–75 kHz). The pixel size is 20 nm. The white color corresponds to the midinfrared absorption signature of single quantum dots. Only a small fraction of the quantum dots can be observed on the image among the ~ 250 quantum dots statistically buried under the surface since all quantum dots are not significantly populated at room temperature as a result of the balance between carrier capture and thermionic emission. Moreover, only a fraction of the quantum dots exhibits an absorption spectrally resonant with the laser wavelength. The typical effective quantum dot size revealed by this measurement is 3–4 pixels, i.e., 60–80 nm. The larger spots are attributed to a gathered group of several dots which cannot be spatially resolved. The

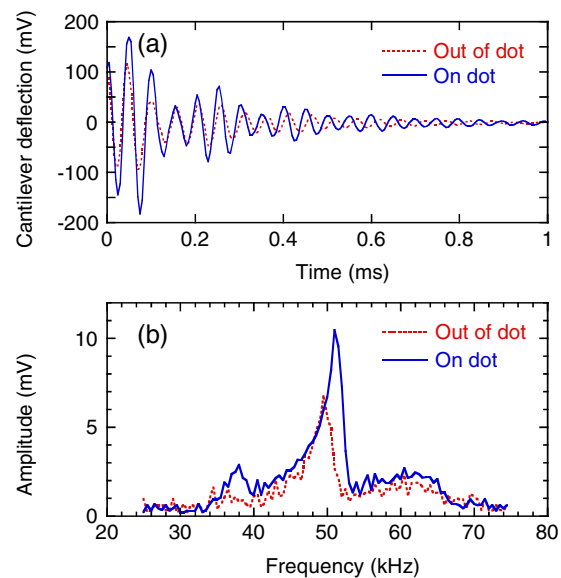


FIG. 2 (color online). (a) Characteristic temporal evolution of the cantilever vibration amplitude with the tip out of an absorbing dot or on top of an absorbing quantum dot. (b) Fourier-transform spectra of the cantilever oscillation.

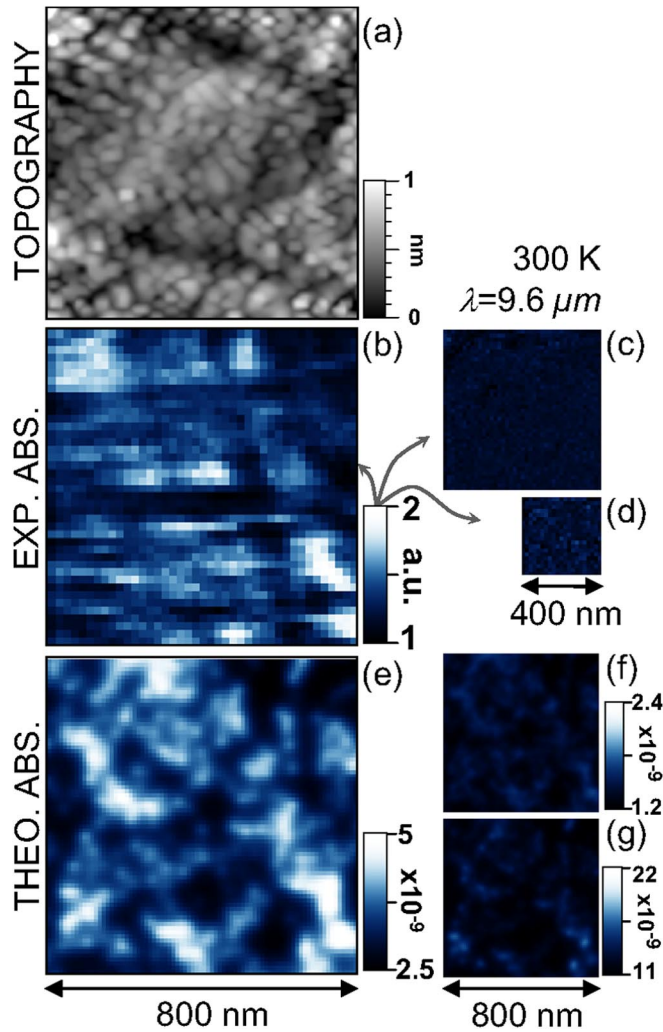


FIG. 3 (color online). (a) $800 \times 800 \text{ nm}^2$ topographic image of sample *S1* surface. (b) $800 \times 800 \text{ nm}^2$ absorption image (41×41 pixels) of the quantum dot sample *S1* doped with a nominal modulation doping of $4 \times 10^{11} \text{ cm}^{-2}$. The excitation wavelength is $9.6 \mu\text{m}$. The quantum dots appear with a bright color. (c) Same measurements on the sample *S0* doped at $4 \times 10^{10} \text{ cm}^{-2}$ and (d) sample *S2* at $4 \times 10^{12} \text{ cm}^{-2}$. (e)–(g) Absorbance simulation corresponding to (b)–(d) doping levels, respectively. The dynamics of the blue scale, i.e., scale maximum over scale minimum, is identical for all absorption images. The scale unit is arbitrary for the cantilever vibration signal (b)–(d), dimensionless for the absorbance reported in (e)–(g).

spatial resolution of the measurement is limited by the depth at which the quantum dot is buried. Considering an isotropic propagation of the deformation field and the thickness $h = 20 \text{ nm}$ of the GaAs covering the quantum dots and the quantum dot diameter $D \sim 20 \text{ nm}$, the effective quantum dot size estimated on the surface is $D + 2\sqrt{2^{2/3} - 1}h \sim 50 \text{ nm}$ close to the observed value. Considering that the optical excitation is around $9.6 \mu\text{m}$, the spatial resolution achieved in this experiment at room temperature is thus around $\lambda/150$. There is clearly a trade-

off between higher resolution and the necessity to cap the quantum dots in order to retain their optical properties. A topographic image of the surface was recorded in contact mode before each spectroscopic measurement, reported for sample *S1* in Fig. 3(a). A small roughness is observed on the sample with an average height of 0.5 nm and a density close to the two-dimensional quantum dot density ($4 \times 10^{10} \text{ cm}^{-2}$). The topographic image thus shows a weak signature of the buried quantum dots. The spectral shift of the AFM cantilever vibration on top of a quantum dot is attributed to the local variation of the roughness which modifies the friction force constant associated with the tip-sample interaction.

In order to exclude any topographic contribution in the image, a sample *S0* nominally doped with $4 \times 10^{10} \text{ cm}^{-2}$ electrons, 10 times less than the previous sample, is considered. Figure 3(c) shows the corresponding midinfrared AFM image ($800 \times 800 \text{ nm}^2$) on the same contrast scale than the one of Fig. 3(b). The image is roughly uniform in this case. For this weakly doped sample, most of the quantum dots are not sufficiently populated to be observed by the AFM technique, the absorbance being below the residual absorption and noise level. This image also indicates that the measurement in Fig. 3(b) is not correlated to topographic artifacts, since both samples have the same nominal structure, i.e., same layer thicknesses, same average dot density, same average dot sizes, geometry, and compositions. A measurement on a higher doped sample [sample *S2*, $4 \times 10^{12} \text{ cm}^{-2}$, Fig. 3(d)] also shows a uniform image associated with the dominant uniform absorption contribution of the free carriers in the continua. The background signal of the measurement [Fig. 2(a) and 2(b)] is attributed to the residual absorption including free carrier absorption and to the additional parasitic signal of neighboring dots. Sample *S1* reveals the presence of about 10 quantum dots under a $800 \times 800 \text{ nm}^2$ surface, a quantum dot being identified by a group of pixels with a signal larger than $1 + 2/3$ times the signal minimum in the image. The experimental images can be modeled by calculating the absorption of each quantum dot of a random distribution and its contribution at the point of detection. The detailed description of this modeling is beyond the scope of this Letter and will be described elsewhere. The calculation of the absorption results from the room temperature electron population of the quantum dots and the absorption cross section. It takes into account the polaron density of states resulting from the strong coupling regime for the electron-phonon interaction [13], a Fermi-Dirac thermal distribution on the levels, the polaron thermionic emission to the continua, the quantum dot absorption cross section, and a random distribution of sizes and spatial positions in the quantum dot plane. Calculated doubly degenerated ground state population is 0.26, 1.2, and 1.9 carriers for samples *S0*, *S1*, and *S2*, respectively. Constant 10^{-9} residual absorbance and standard free carrier absorp-

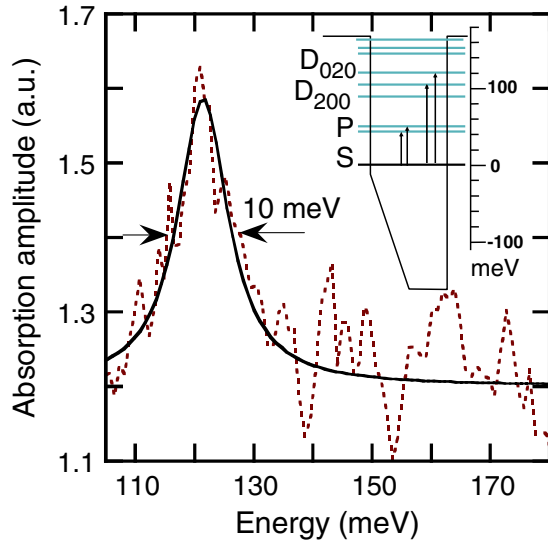


FIG. 4 (color online). Spectral dependence of a single quantum dot intersublevel absorption at room temperature. The dashed line represents the experimental data points. The full line is the Lorentzian line shape best fitting the data. The inset shows the electronic structure of a single self-assembled quantum dot.

tions of the electrons in the continua are accounted for. Each quantum dot is supposed to emit a spherical deformation wave towards the surface, with a tip-collected energy proportional to the local sheet energy density on the surface. Typical results corresponding to Fig. 3(b)–3(d) are shown in Fig. 3(e)–3(g), respectively. Note that the image contrasts from one doping level to the next vary consistently with experiment. The image of Fig. 3(b) corresponds in the simulation Fig. 3(e) to an average population of $1.2^{+0.5}_{-0.4}$ carriers in the S ground states, accounting for the statistical fluctuation of parameters for a probed area of fixed size. It indicates that only a small fraction of the carriers provided by the doping is actually available for the quantum dot absorption at room temperature and that these carriers are nonuniformly distributed in the quantum dots. The images thus provide spatial information on the quantum dot population distribution at room temperature.

The spectral dependence of the absorption of a single quantum dot for a fixed position of the AFM tip is reported in Fig. 4 by scanning the wavelength of the free-electron laser. The measured signal is proportional to the total local absorption, i.e., quantum dots plus background absorption, and to the square of the local electric field sensible to Fabry-Perot effects. The vibration spectra was therefore normalized for each wavelength by a reference spectra taken out of a significantly populated quantum dot. The single dot absorption is resonant around 120 meV with a Lorentzian linewidth of 10 meV. At room temperature, the quantum dots which are significantly populated are the large quantum dots of the inhomogeneous distribution, i.e., corresponding to the deepest confined states. The

quantum dot electronic structure is calculated by solving the three-dimensional strain dependent Pidgeon-Brown Schrödinger equation written in 8 band $\mathbf{k} \cdot \mathbf{p}$ formalism [11] accounting for the quantum dot geometry and composition profile. Resonant absorptions with dipole moments along the z direction are predicted around 100–120 meV. The calculation indicates that for large quantum dots, the observed absorption at 120 meV corresponds to one of the two S - D bound-to-bound intersublevel absorptions exhibiting a nonvanishing dipole. Its linewidth is given by the homogeneous linewidth. The corresponding short dephasing time ($T_2 \sim 130$ fs), well below the relaxation time measured for quantum dots following an intersublevel excitation [11], is attributed to scattering due to the large number of carriers present in the wetting layer and the quantum dot surrounding since the excited final state in this experiment has a significant overlap with the barrier states and is not as well confined as the ground state. Similar linewidths (~ 10 meV) have been reported for interband transitions in photoluminescence experiments at room temperature [14], making the observation of interband absorption of a single quantum dot at room temperature very challenging. The presented technique can be adapted to study at room temperature the interband quantum dot absorption characterized by typical dipole lengths of 0.6 nm. Finally, this work corresponds to the first generation and local detection of phonons emitted by semiconductor quantum dots.

*philippe.boucaud@ief.u-psud.fr

†sebastien.sauvage@ief.u-psud.fr

- [1] *Single Quantum Dots: Fundamentals, Applications and New Concepts*, edited by P. Michler, Editor Topics in Applied Physics Vol. 90 (Springer, New York, 2003).
- [2] M. Kroutvar *et al.*, *Nature (London)* **432**, 81 (2004).
- [3] H. Hess *et al.*, *Science* **264**, 1740 (1994).
- [4] J. R. Guest *et al.*, *Science* **293**, 2224 (2001).
- [5] B. Alen *et al.*, *Appl. Phys. Lett.* **83**, 2235 (2003).
- [6] K. Karrai and R. J. Warburton, *Superlattices Microstruct.* **33**, 311 (2003).
- [7] B. Knoll and F. Keilmann, *Nature (London)* **399**, 134 (1999).
- [8] M. Fricke *et al.*, *Europhys. Lett.* **36**, 197 (1996).
- [9] This dipole length is an upper limit for the S - D transition oscillator strength observed by midinfrared absorption spectroscopy in n -doped InAs/GaAs quantum dot ensembles.
- [10] A. Dazzi, R. Prazeres, F. Glotin, and J.-M. Ortega, *Ultramicroscopy* **107**, 1194 (2007).
- [11] P. Boucaud and S. Sauvage, *C.R. Physique* **4**, 1133 (2003).
- [12] C. Thomsen, H. T. Grahn, H. J. Maris, and J. Tauc, *Phys. Rev. B* **34**, 4129 (1986).
- [13] S. Hameau *et al.*, *Phys. Rev. Lett.* **83**, 4152 (1999).
- [14] K. Matsuda, T. Saiki, H. Saito, and K. Nishi, *Appl. Phys. Lett.* **76**, 73 (2000).